Reports in Mechanical Engineering
Vol. 7, No. 2, 2026, pp. 81-96
ISSN: 2683-5894, DOI: https://doi.org/10.5281/zenodo.22660387

Rarefied Flow and Heat Transfer of Thermo-Responsive Al_2O_3/TiO_2/Ag–PNIPAm Tri-Hybrid Nanofluids in Microchannels: An MRT-LBM Study

Zainab Kadhim Al-Khazragie[1*], Jaafar Albadr[1], Ali Sami Hashem[1]
[1]Department of Gass Processes and Petrochemicals, College of Oil and Gas, Basra University for Oil and Gas, Iraq

Article Info

Article history:

Received April 10, 2026
Revised June 16, 2026
Accepted July 19, 2026

Keywords:

Tri-Hybrid Nanofluid,
Smart Responsive Polymer,
PNIPAm,
LCST,
Rarefied Flow,
Knudsen Number,
Velocity Slip,
Temperature Jump,
Microchannel Heat Transfer,
Lattice Boltzmann Method,
FENE-P,
Non-Newtonian Nanofluids,
Al_2O_3/TiO_2/Ag

ABSTRACT

The rapid miniaturization of thermal-management systems and microfluidic devices has intensified the need to understand fluid transport at scales where classical continuum assumptions break down. This paper presents the first comprehensive investigation of rarefied flow and heat transfer in microchannels laden with a novel smart thermo-responsive tri-hybrid nanofluid composed of aluminium oxide (Al_2O_3), titanium dioxide (TiO_2), and silver (Ag) nanoparticles dispersed in an aqueous poly(N-isopropylacrylamide) (PNIPAm) solution. PNIPAm undergoes a well-characterized lower critical solution temperature (LCST) transition at approximately 32°C, inducing a reversible coil-to-globule conformational change that dramatically alters the suspension viscosity and thermal conductivity in a temperature-driven, self-regulating manner. This work addresses the unexplored coupling between stimuli-responsive rheology, tri-hybrid nanoparticle synergy, and rarefaction-induced velocity slip and temperature jump at the solid–fluid interface. Knudsen-number-corrected Navier–Stokes equations, augmented with second-order Maxwell–von Smoluchowski slip/jump boundary conditions, are coupled with FENE-P viscoelastic constitutive equations that incorporate a temperature-dependent relaxation time $\lambda_p(T)$ capturing the PNIPAm LCST transition. Tri-hybrid effective thermophysical properties are computed via extended Hamilton–Crosser and modified Krieger–Dougherty mixture models accounting for nanoparticle morphology, interfacial nanolayer resistance, and Brownian diffusion contributions from all three nanoparticle species. Numerical simulations are performed using a Multiple-Relaxation-Time Lattice Boltzmann Method (MRT-LBM) with polymer stress forcing and cross-validated against finite-volume CFD (ANSYS Fluent with user-defined functions). Parametric studies span Knudsen numbers Kn = 0.001–0.1 (slip-flow regime), total nanoparticle volume fractions φ = 0–6%, PNIPAm concentration c_p = 0–2000 ppm, Reynolds numbers Re = 1–100, and wall temperatures Tc = 25–45°C, which straddle the PNIPAm LCST. Results reveal a pronounced non-monotonic Nusselt number response to wall temperature: below the LCST (Tc < 32°C), PNIPAm chains remain hydrophilic and extended (high viscosity, moderate thermal conductivity), while above the LCST (Tc > 32°C), the collapsed globular conformation reduces viscosity and activates a self-regulating heat-transfer enhancement mechanism. The tri-hybrid combination delivers a 41.6% higher effective thermal conductivity than single-component Al_2O_3 at φ = 3%, owing to phonon-scattering complementarity between the three nanoparticle species. Net thermal performance gains of up to 47.3% relative to the pure-liquid slip-flow baseline are demonstrated at optimum conditions (Kn = 0.01, φ = 3%, c_p = 600 ppm, Tc = 36°C). These findings establish design guidelines for smart, self-regulating polymer-nanofluid-cooled MEMS, microreactors, and biomedical lab-on-chip platforms.

Corresponding Author:

Zainab Kadhim Al-Khazragie
Department of Gass Processes and Petrochemicals, College of Oil and Gas, Basra University for Oil and Gas
Email: zainab.alkhazragie@buog.edu.iq

1. Introduction

Micro-system technologies, including Micro-electro-mechanical systems (MEMS), microreactor engineering, medical lab-on-chip platforms and next-generation electronic cooling, have increasing requirements for thermal loads that require greater performance from their thermodynamic components as space available for flow decreases (Kunze et al., 2024). With the hydraulic diameters of these elements reduced to less than 100 μm, the ratio of the mean free path of a fluid molecule (λ) to the dimension of the channel (L), i.e. λ/L—also referred to as the Knudsen number—becomes large enough that the traditional no-slip/no-temperature-jump boundary conditions observed with traditional fluid mechanics can no longer be regarded as accurate at this scale (Agarwal et al., 2023; Le & Roohi, 2015). In the slip flow regime ($0.001 \leq Kn \leq 0.1$), the interaction of fluid molecules with the solid surface has a time scale on the order of the molecular relaxation time, resulting in significant tangential velocity slip and thermal resistance at the wall of the channel that impacts pressure drop, velocity profiles and Nusselt number distributions. Thus, accurate prediction of these effects is essential for the reliable design of next-generation miniaturized thermal systems.

As with many geometric problems, there are also various ways to enhance the thermal performance of conventional coolants such as water through new nanofluid technology (suspensions of nano-sized (<100 nm) metal or ceramic particles in a base liquid) (Choi, 1995). The evolution of these products has already moved from the earlier formulations of binary (one type of nanoparticle) to more advanced hybrid and tri-hybrid forms (in which three different types of nanoparticles are dispersed together) where enhanced thermal conductivity is achieved through complementary phonon scattering, surface area, and interfacial energy mechanisms that cannot all occur at the same time with only one type of particle used in a single-nanoparticle suspension (Suresh, Venkitaraj, & Selvakumar, 2011; Suresh, Venkitaraj, Selvakumar, et al., 2011). For example, aluminum oxide (Al_2O_3) provides long-term chemical stability with moderate enhancement of thermal conductivity, titanium dioxide (TiO_2) provides photocatalytic and anti-agglomeration properties to the nanofluid, and silver (Ag) has the highest ever-reported intrinsic thermal conductivity of a commercial metallic nanoparticle at (429 W m^{-1} K^{-1}) as measured on a quantum scale (<100 nm) where quantum confinement does not exist (Sahoo & Kumar, 2020). In addition, the development of advanced tri-hybrid nanofluids has shown that the effective thermal conductivity provided by this combination of nanoparticles is greater than predicted by simply adding the intrinsic conductivities of each unique nanoparticle and has been attributed to improved interfacial phonon coupling and the formation of nanoparticle clusters when mixed (I. L. Animasaun et al., 2022).

The interface of these novel developments is a critically underexplored area: using stimulus-responsive, or 'smart', polymers as the base-fluid matrix. The most widely studied thermo-responsive polymer is poly(N-isopropylacrylamide) or PNIPAm, which exhibits a very sharp and very reversible lower critical solution temperature (LCST) transition at approximately $T\_LCST \approx 32°C$ in aqueous solution (Schild, 1992). Below the LCST, PNIPAm chains exist in a hydrophilic coil (extended) conformation because of strong hydrogen-bonding interactions with water and thus have relatively high viscosity and moderate elasticity. Above the LCST, the increased entropic penalty of partially ordering water around the isopropyl group causes the PNIPAm chains to undergo a cooperative transition from an extended conformation to a globular conformation, resulting in the release of water from the bulk, a significant decrease in the effective hydrodynamic radius, a dramatic decrease in the viscosity, and an increase in heat absorption due to phase transition. This thermo-responsive rheological transition is triggered by the very thermal load the fluid was designed to manage and creates a thermal management system that is inherently self-regulating with attributes that are unattainable with conventional polymer additives (Nayak & Lyon, 2005). When tri-hybrid nanoparticles are dispersed in the PNIPAm matrix, the resulting smart nanofluid benefits from both nanoscale thermal-conductivity enhancement due to the nanoparticles and flow control due to the polymer, as both mechanisms are influenced by local temperature.

Although these research areas have received much attention individually, there has yet to be a study that has combined (i) tri-hybrid nanoparticle interaction effects, (ii) smart thermo-responsive polymer viscoelastic responses, and (iii) the effect of rarefaction-induced slip and temperature jump on materials at the micro-scale. This is largely due to previous analyses either treating the nanofluid as a single-phase Newtonian media while including slip effects (Zarita & Hachemi, 2019) or analyzing hybrid or polymer nanofluids with non-Newtonian behavior while ignoring the effects of continuum breakdown in the analysis of macro-scale channels (Tawalbeh et al., 2024). In addition, the limited literature available on bi-hybrid nanofluids subjected to slip-flow through micro-channels (Jamshed et al., 2021) does not include an examination of the viscoelastic behavior of polymers, nor does any examine the behavior of thermo-responsive PNIPAm polymer chains. This paper addresses these significant gaps by presenting a common mathematical and numerical method that simultaneously encompasses all three areas of scientific investigation (Sharipov, 2011).

This paper presents several unique contributions to the existing literature, which include: (1) developing and validating a coupled FENE-P/PNIPAm constitutive model with temperature-dependant LCST kinetics defined in a

Knudsen-corrected Navier–Stokes framework; (2) creating extended Hamilton–Crosser tri-hybrid effective property correlations of the $Al_2O_3/TiO_2/Ag$ ternary nanoparticle system, incorporating particle shape/size polydispersity and nanolayer resistance; (3) the first implementation of MRT-LBM with tri-hybrid nanofluids and FENE-P polymer forcing under slip flow boundary conditions; (4) identifying and quantifying LCST-induced self-regulating heat transfer mechanisms in the slip flow regime, which are fundamentally new physical phenomena; and (5) providing Kn - φ - cp - Tc design maps for engineers to directly select operating conditions that optimally achieve thermal performance, without having to simulate each case. The paper is structured as follows: Section 2 provides a literature review, Section 3 presents the complete mathematical formulation, Section 4 discusses the numerical methodologies used to conduct the research, Section 5 presents and discusses results from a parametric study conducted during the research, and Section 6 provides concluding remarks and engineering recommendations.

2. Literature Review

2.1 Rarefaction and Slip-Flow Physics in Microchannels

Karniadakis et al. (2005) established the classical framework for the study of rarefied gas and liquid sequences experimentally through comprehensive methods including the identification of four Knudsen number regions: continuum ($Kn < 0.001$), slip-flow ($0.001 \leq Kn \leq 0.1$), transition ($0.1 < Kn \leq 10$) and free-molecular ($Kn > 10$); and the definition of boundary conditions for higher-order velocity-slip. Kolachev studied gas-microfluidic flow in detail to assess first-order slip-model accuracy through experimental and theoretical investigations of accommodation coefficients related to tangential momentum transfer at solid surfaces. Essentially, these studies by Arkilic et al. (1997) and Kunze et al. (2024) broadened the range of Knudsen numbers measured for functional nanostructured surfaces, yielding valuable insight into how chemical properties affect accommodation coefficients and effective slip lengths.

The source of liquid velocity slip originates from the interaction of molecules on surfaces, as opposed to gas kinetic rarefaction, but mathematically speaking the slip boundary conditions are still formally equivalent (Ho & Tai, 1998). Duan and Muzychka (2010) showed that slip corrections beyond first order must be used in the hydrodynamic entrance region of non-circular micro-channels. The second-order temperature-jump boundary condition derived by Le and Roohi (2015) predicts Nusselt numbers within 3% of DSMC data for the complete slip-flow regime and was used in this work. Tantos, Varoutis, and Day (Ebrahimi & Roohi, 2017) used DSMC to characterise rarefied flow across the full slip-to-free-molecular transition in divergent micro- and nano-channels, providing an excellent source of authoritative validation data. Agarwal et al. (2023) reviewed Maxwell's velocity-slip and temperature-jump models from first-order to recent higher-order and nonlinear extensions and confirmed that second-order models are sufficient and necessary for the slip-flow regime targeted by this work.

2.2 Hybrid and Tri-Hybrid Nanofluid Thermal Conductivity Enhancement

The book by Choi (1995) led to an increase in research on the thermal-conductivity enhancement of metallic nanoparticle dispersions, which continued for more than 20 years. The development from single-component to multiple-component mixtures of nanoparticles was based on theoretical predictions demonstrating that mixing two or more particles with different crystallographic structures, surface energies, and phonon dispersion relations could provide a greater thermal conductivity than simply mixing the two nanoparticles using simple mixing rules (Suresh, Venkitaraj, Selvakumar, et al., 2011). Suresh, Venkitaraj and Selvakumar (2011) studied hybrid nanofluids that combined Al_2O_3 and Cu nanoparticles . Suresh, Venkitaraj and Selvakumar (2011) reported that the hybrid nanofluids exhibited up to 29.1% greater thermal conductivity than the single-component Al_2O_3 hybrid nanofluids at the same mass fraction ($\varphi = 2\%$) and that the additional thermal conductivity was due to Cu-mediated interfacial phonon coupling, which resulted in a 63% synergy premium. Sundar et al. (2017) studied hybrid nanofluids containing ND-Ni and ND-Co. They found that adding magnetic nanoparticles provided an additional enhancement from Lorentz-force convection effects not available from thermal-conductivity enhancement alone.

Recently, tri-hybrid nanofluids have emerged as a promising approach to simultaneously improving thermal conductivity, viscosity, and dispersion stability. Sahoo and Kumar (2020) investigated $Al_2O_3/TiO_2/SiO_2$ tri-hybrid nanofluids and reported a 31.6% enhancement in thermal conductivity at $\varphi = 0.1\%$, significantly exceeding that of binary nanofluids. Adding metal Ag nanoparticles to oxide tri-hybrid systems has a particularly synergistic effect because Ag provides ballistic heat conduction due to its high phonon mean free path, while oxide nanoparticles create interfacial thermal resistance networks that enhance the overall effective medium conductivity via anomalous conduction (I. L. Animasaun et al., 2022). There is still ongoing research into effective property correlations for tri-hybrid nanofluids; however, the most cited correlation to date is (I. Animasaun et al., 2022) extended Hamilton-Crosser model. This study extends the Hamilton-Crosser model to account for the viscosity of a PNIPAm matrix, as well as the thermal boundary resistance due to a nanolayer at the interface of each nanoparticle.

2.3 Smart Thermo-Responsive Polymer Nanofluids

Schild (1992) conducted an extensive investigation of the LCST (approximately 32°C) of PNIPAm in solution at the molecular level; he found that the coil-to-globule transition is primarily an entropic phenomenon driven by the balance between hydrophilic amide-water hydrogen bonding and hydrophobic isopropyl-water contributions. The transition is approximately 2-3°Cover a molecular range (10-200 kDa) of linear PNIPAm and can be altered through copolymerization. Pelton (2000) showed that PNIPAm microgel particles undergo up to a 40-fold reversible volume change at the LCST, resulting in a 2-order-of-magnitude change in effective viscosity and making PNIPAm fluids highly sensitive thermo-rheological materials.

The combination of PNIPAm and NP has created further complexity. Nayak and Lyon (2005) demonstrated that adding Ag NPs to PNIPAm chains shifted the LCST by as much as 4°C due to steric and surface-energy effects. In addition, they reported that NPs also improved the thermal conductivity of the collapsed globule state by 1.8 times compared to the thermal conductivity of the pure polymer solution—a behavior that does not exist in conventional polymer–nanoparticle mixtures. Khan et al. (2024) reported that the volume fraction of NPs enhances the elastic normal stresses of the polymer, which increases the rate of the shear-thinning transition using the FENE-P constitutive equations. Additionally, at Kn > 0, shear rate increases induced by rarefaction in the vicinity of a wall further increase the magnitude of this coupling by extending polymer chains beyond their original equilibrium LCST response. Importantly, to date, no studies have correlated FENE-P polymer-chain dynamics with the LCST kinetics of PNIPAm, or considered the contributions of tri-hybrid NPs and Knudsen-corrected slip conditions in microchannels—this is the novel contribution of this paper.

2.4 Lattice Boltzmann Method for Non-Newtonian Nanofluid Slip Flows

Because of its basis in kinetic theory, the Lattice Boltzmann Method (LBM) connects continuum-space and molecular-space naturally applying to slip-flow regimes (Succi, 2002). It was shown by Succi (2002) that a scheme consisting of suitable bounce-back conditions recovers the first order velocity slip of a fluid in accordance with Maxwell's accommodation model. Nie et al. (2002) modified boundary conditions within the LBM to extend it to second-order slip flows. The D2Q9 LBM using BGK approximation with a single-relaxation-time (SRT) collision operator has been extensively validated against Navier-Stokes solutions within nanofluid applications (Xuan & Yao, 2005). The Multiple-Relaxation-Time (MRT) extension of this collision operator, where each hydrodynamic moment is allowed to relax at its own independent rate, provides significant benefits relative to numerical stability/accuracy of computational results for viscoelastic fluids at high Weissenberg numbers (Lallemand & Luo, 2000), making it advantageous for this current polymer/nanofluid system.

In their research on LBM using water/Ag nanofluids in microchannels with 1st order slip and jump boundary conditions, Zarita and Hachemi (2019) found that when φ increases, so does the Nusselt number (Nu), but the Knudsen number (Kn) has an opposite effect. In their work, Moshfegh et al. (2020) extended LBM analysis of hydrophobic microchannels under magnetic fields to include wall-slip effects due to interactions between nanoscale particles and wall surfaces. However, all prior LBM studies have used Newtonian base fluids. This study expands the application of the MRT-LBM scheme to a non-Newtonian polymer nano-hybrid fluid system composed of PNIPAm, Ag, MgO, and SiO2. To account for polymer stress effects on fluid motion (as a body force), we will use a FENE-P constitutive model along with the Guo boundary condition to model Knudsen-layer-resolved slip at the walls. Finally, the new combined bounce-back/specular reflection (CBBSR) approach will be developed and applied to model this complex flow field.

3. Mathematical Formulation

3.1 Flow Regime Characterization

The local Knudsen number is defined as $Kn = \frac{\lambda_{eff}}{D_h}$, where λ_{eff} is the effective mean free path of the PNIPAm–tri-hybrid nanofluid mixture and D_h is the microchannel hydraulic diameter. For liquid-phase slip flows, λ_{eff} is evaluated via the molecular-scale shear-wave propagation model of Ho and Tai (1998):

$$\lambda_{eff} = \frac{\mu_{eff}}{(\rho_{eff} \cdot \alpha_s)}$$

where α_s is the thermal diffusivity of the mixture and μ_{eff} is the effective dynamic viscosity accounting for both PNIPAm viscoelasticity and tri-hybrid nanoparticle contributions (Section 3.4). This definition of λ_{eff} captures the temperature dependence of the mean free path through both $\mu_{eff(T)}$ and $\alpha_{s(T)}$, including the abrupt variation across

the PNIPAm LCST transition. The present study targets the slip-flow regime $0.001 \leq \mathrm{Kn} \leq 0.1$.

Flow regimes are further characterized by: the Reynolds number $Re = \frac{\rho_{eff} U_{in} D_h}{\mu_{eff}}$; the Weissenberg number $Wi = \lambda_p \frac{(T) U_{in}}{D_h}$, representing the ratio of the temperature-dependent PNIPAm relaxation time to the convective timescale; and the Péclet number $Pe = Re \cdot \Pr_{eff}$. The Weissenberg number is a key non-dimensional parameter because Wi > 1 signals onset of elastic instabilities in which polymer chain stretching begins to influence macroscale flow patterns, a condition reached near the LCST transition in the present system.

3.2 Governing Equations — Modified Navier–Stokes System

The steady, incompressible, laminar flow of the PNIPAm–the following system of conservation equations governs tri-hybrid nanofluid mixture:

Continuity:

$$\nabla \cdot u = 0$$

Momentum:

$$\rho_{eff}(u \cdot \nabla)u = -\nabla p + \nabla \cdot [\tau_N + \tau_P] + \rho_{eff} g$$

Energy:

$$\rho_{eff} c_{\{p,eff\}(u \cdot \nabla)T} = \nabla \cdot \left(k_{eff} \nabla T\right) + \Phi_{visc} + Q_{LCST}$$

where $\tau_N = \mu_{s(\nabla u + \nabla u^{\mathrm{T}})}$ is the Newtonian (solvent) contribution to the stress tensor with solvent viscosity μ_s, τ_P is the viscoelastic polymer stress governed by the FENE-P constitutive equation (Section 3.3), $\Phi_{visc} = \tau : (\nabla u)$ is the viscous dissipation, which becomes significant at elevated Weissenberg numbers and high heat fluxes, and Q_{LCST} is a volumetric heat source/sink term representing the latent enthalpy of the PNIPAm coil-to-globule transition:

$$Q_{LCST} = -c_p \cdot \Delta H_{LCST} \cdot \frac{d\alpha_{PNIPAm}}{dt}$$

Here $\Delta H_{LCST} \approx 6.7\ kJ\ mol^{-1}$ is the molar enthalpy of the LCST transition [9], $\alpha_{PNIPAm} \in [0,1]$ is the degree of PNIPAm collapse, and c_p is the polymer molar concentration. This term acts as a thermal buffer: when the local temperature crosses $T_{LCST} = 32°C$, heat is absorbed (ΔH > 0, Q_LCST < 0), reducing the local temperature and partially suppressing wall overheating—the self-regulating mechanism identified in this work.

3.3 PNIPAm Smart Polymer Constitutive Model (FENE-P with LCST Kinetics)

The PNIPAm polymer contribution to the stress tensor is governed by the Finitely Extensible Nonlinear Elastic–Peterlin (FENE-P) constitutive equation, extended here with a temperature-dependent relaxation time that captures the LCST transition:

$$\tau_P + \lambda_{p(T)[\tau^{\mathrm{T}}{}_P + f(C)\tau_P]} = \mu_p f(C)(\nabla u + \nabla u^{\mathrm{T}})$$

where $\tau^{\mathrm{T}}{}_P$ is the upper-convected derivative of the polymer stress, $f(C) = \frac{1}{1 - \frac{tr(C)}{L^2}}$ is the FENE-P spring force factor, C is the polymer conformation tensor, L is the maximum chain extensibility (L = 100 for PNIPAm of molecular weight 70 kDa (Khan et al., 2024)), and μ_p is the polymer contribution viscosity. The temperature-dependent PNIPAm relaxation time $\lambda_p(T)$ is modeled via a modified Williams–Landel–Ferry (WLF) equation incorporating the LCST sigmoid:

$$\lambda_{p(T)} = \lambda_p, 0 \cdot \exp\left(-\frac{E_a}{R} \cdot \left[\frac{1}{T} - \frac{1}{T_{ref}}\right]\right) \cdot \left[1 - \alpha_{PNIPAm(T)}\right]$$

where $\lambda_{\{p,0\}}$ is the reference relaxation time at $T_{ref} = 298\ K, E_a$ is the activation energy for chain disentanglement, R is the universal gas constant, and the factor $(1 - \alpha_{\{PNIPAm\}})$ accounts for the reduction in chain interaction length as globules form above the LCST. The degree of PNIPAm collapse $\alpha_{\{PNIPAm\}}$ follows a cooperative sigmoid transition function:

$$\alpha_{PNIPAm(T)} = \frac{1}{\left\{1 + \exp\left[-n_H \cdot \frac{T - T_{LCST}}{T_{LCST}}\right]\right\}}$$

where n_H is the Hill cooperativity coefficient (~15–18 for linear PNIPAm (Pelton, 2000)), governing the sharpness of the LCST transition. This formulation continuously and differentiable transitions the polymer from fully coiled (extended FENE-P with high λ_p) below the LCST to fully collapsed (elastic contribution vanishes, $\lambda_p \rightarrow 0$) above the LCST, consistent with experimental observations (Nayak & Lyon, 2005; Schild, 1992).

3.4 Tri-Hybrid Effective Thermophysical Properties

The tri-hybrid nanofluid effective thermophysical properties are computed using extended mixture models for the three-component $Al_2O_3/TiO_2/Ag - PNIPAm$ system. The total volume fraction is φ = φ₁ + φ₂ + φ₃, with individual volume fractions maintained at a 40:40:20 mass ratio (Al_2O_3: TiO_2: Ag) to balance stability, conductivity, and cost (Sahoo & Kumar, 2020).

Effective dynamic viscosity follows the Krieger–Dougherty extension for polydisperse particle mixtures, modified for the PNIPAm LCST transition:

$$\mu_{eff} = \mu_{\{base\}(T,\dot{\gamma},c_p)} \times \prod_{\{i=1\}}^{\{3\}} \left(1 - \frac{\varphi_i}{\varphi_{\{max,i\}}}\right)^{\left\{-2.5\varphi_{\{max,i\}}\right\}}$$

where $\mu_{\{base\}(T,\dot{\gamma},c_p)}$ is the PNIPAm solution viscosity as a function of temperature T, shear rate $\dot{\gamma}$, and polymer concentration c_p, correlated via the Carreau–Yasuda model with temperature-dependent zero-shear viscosity $\eta_{0(T)}$ that incorporates the LCST sigmoid. The maximum packing fraction $\varphi_{\{max,i\}}$r each particle species is computed from a random-close-packing model accounting for the actual particle size ratio.

The effective thermal conductivity is computed via the extended Hamilton–Crosser model for tri-hybrid nanofluids, corrected for interfacial nanolayer thermal resistance using the series–parallel network approach of Levin and Miller (1981):

$$k_{eff} = k_f \times \left\{ \frac{\left[\Sigma_{\{i=1\}}^{\{3\}}\left(\frac{\varphi_i}{\varphi}\right) \cdot k_{\{np,i\}} + 2k_f - 2\Sigma\varphi_i\left(k_f - k_{\{np,i\}}\right)\right]}{\left[\Sigma_{\{i=1\}}^{\{3\}}\left(\frac{\varphi_i}{\varphi}\right) \cdot k_{\{np,i\}} + 2k_f + \Sigma\varphi_i\left(k_f - k_{\{np,i\}}\right)\right]} \right\} \times \left(1 + A\varphi^B \cdot Pe_{\{np\}}^C\right)$$

where $k_{\{np,i\}}$ are the bulk thermal conductivities of Al_2O_3 (40 W m⁻¹ K⁻¹), TiO_2 ($8.4\ W\ m^{-1}K^{-1}$), and Ag ($429\ W\ m^{-1}\ K^{-1}$), respectively; $Pe_{\{np\}} = \frac{u_B d_p}{\alpha_f}$is the nanoparticle Péclet number with u_B the Brownian velocity; and A = 23.2, B = 2.5, C = 0.4 are empirical constants calibrated against molecular dynamics simulation data for ternary nanoparticle suspensions (I. Animasaun et al., 2022). The PNIPAm matrix thermal conductivity k_f varies with the LCST transition state, increasing by approximately 18% upon collapse due to reduced polymer–water interface area and associated phonon-scattering reduction (Nayak & Lyon, 2005).

The effective specific heat and density are computed from standard volumetric mixing rules:

$$\rho_{eff} = (1-\varphi)\rho_f + \Sigma_{\{i=1\}_i^{\{3\}\varphi}} \rho_{\{np,i\}}$$

$$\left(\rho c_p\right)_{eff} = (1-\varphi)\left(\rho c_p\right)_f + \Sigma_{\{i=1\}_i^{\{3\}\varphi}} \left(\rho c_p\right)_{\{np,i\}}$$

Table 1 summarises the nanoparticle thermophysical properties used in all simulations.

Table 1: Thermophysical Properties of Nanoparticle Species at T = 300 K

Property	Al_2O_3	TiO_2	Ag	PNIPAm–H_2O (Coil)	Ref.
$\rho\ (kg\ m^{-3})$	3970	4250	10500	1010	I. L. Animasaun et al. (2022); Sahoo and Kumar (2020)
$c_p (J\ kg^{-1}K^{-1})$	765	686	235	4100	I. L. Animasaun et al. (2022); Sahoo and Kumar (2020)
$k\ (W\ m^{-1}K^{-1})$	40.0	8.40	429	0.598	I. L. Animasaun et al. (2022); Sahoo and Kumar (2020)
$d_p (nm)$	30	25	15	—	I. L. Animasaun et al. (2022); Sahoo and Kumar (2020)
$Shape\ factor\ n_H$	3.0 (sphere)	3.0 (sphere)	3.0 (sphere)	—	I. Animasaun et al. (2022)

3.5 Knudsen-Corrected Slip-Flow Boundary Conditions

At the microchannel walls, second-order Maxwell–von Smoluchowski boundary conditions are imposed, extended to account for the non-Newtonian effective viscosity of the polymer-nanofluid:

Velocity slip:

$$u_{slip} = \left[\frac{2-\sigma_v}{\sigma_v}\right] \cdot Kn \cdot \left(\frac{\partial u}{\partial n}\right)_{wall} + \left[\frac{2-\sigma_v}{\sigma_v}\right] \cdot \left(\frac{Kn^2}{2}\right) \cdot \left(\frac{\partial^2 u}{\partial n^2}\right)_{wall}$$

Temperature jump:

$$T_{jump} = \left[\frac{2-\sigma_T}{\sigma_T}\right] \cdot \left[\frac{2\gamma}{\gamma+1}\right] \cdot \left(\frac{Kn}{\Pr_{eff}}\right) \cdot \left(\frac{\partial T}{\partial n}\right)_{wall}$$

where σ_v and σ_T are the tangential momentum and thermal accommodation coefficients, respectively (baseline values $\sigma_v = \sigma_T = 0.85$, with parametric variation from 0.6 to 1.0); γ is the isentropic exponent; and n is the outward wall-normal coordinate. A critical modification introduced in the present work concerns the temperature dependence of the effective Prandtl number $\Pr_{eff} = \frac{\mu_{eff} c_{\{p,eff\}}}{k_{eff}}$ that appears in the temperature-jump condition. Because $\Pr_{eff}$ varies abruptly at the PNIPAm LCST, the temperature-jump magnitude is itself a non-monotonic function of wall temperature, contributing to the self-regulating thermal performance mechanism described in Section 5.3.

3.6 MRT-LBM Formulation with Polymer Stress Forcing

The D2Q9 Multiple-Relaxation-Time Lattice Boltzmann scheme solves the discrete Boltzmann equation in moment space:

$$f_{i(x + e_{i\delta t}, t + \delta t)} - f_{i(x,t)} = -M^{-1} S \left[m - m^{eq}\right]_i + M^{-1}\left(I - \frac{S}{2}\right) F_i \mathrm{c}$$

where f_i are particle distribution functions for the i-th discrete velocity direction, e_i are the D2Q9 lattice velocity vectors, M is the 9×9 orthogonal transformation matrix mapping distribution functions to moment space, $S = diag(s_0, s_1, \ldots, s_8)$ is the diagonal relaxation matrix, and $m = Mf, m^{eq} = Mf^{eq}$ are the actual and equilibrium moment vectors. The MRT relaxation rates are tuned to minimize numerical dispersion while ensuring that effective kinematic viscosity recovers the polymer-nanofluid value: $s_v = \frac{1}{\frac{3\nu_{eff}\delta t}{\delta x^2} + 0.5}$.

The tri-hybrid nanofluid effective thermophysical properties enter through the equilibrium distribution functions f_i^{eq} and through modification of the energy relaxation rate $s_k = \frac{1}{\frac{6\alpha_{eff}\delta t}{\delta x^2} + 0.5}$. The polymer stress contribution τ_P, computed from the FENE-P conformation tensor equation, enters as a body-force term via the modified Guo forcing scheme:

$$F_i = \frac{w_i (e_{\{i\alpha\}} - u_\alpha)}{c_s^2} \times \left[\frac{\partial_\beta \tau_{\{P,\alpha\beta\}}}{\rho_{eff}} + \gamma_\alpha\right]$$

where w_i are the D2Q9 weights, $c_s = \frac{1}{\sqrt{3}} \cdot \frac{\delta x}{\delta t}$ is the LBM lattice speed of sound, and γ_α represents gravitational and other body forces. The FENE-P conformation tensor equation is solved in parallel using a second-order operator-splitting scheme, updating C at each LBM timestep. Knudsen-number-dependent velocity slip is implemented at solid boundaries through the combined bounce-back/specular-reflection (CBBSR) scheme with reflection coefficient:

$$r = \frac{\left(Kn - \frac{1}{12}\right)}{\left(Kn + \frac{1}{12}\right)}$$

which continuously interpolates between pure bounce-back (r = 0, no-slip, Kn → 0) and pure specular reflection (r = 1, full-slip, Kn → ∞), consistent with the Knudsen-layer physics of the slip-flow regime.

4. Numerical Methodology

4.1 Computational Domain and Boundary Conditions

The microchannel geometry is defined as an aspect ratio of L = 500 μm and hydraulic diameter of D_h = 10 μm. This value allows for fully developed flow to occur in the channel ($i.e. L_h \approx 0.05 \cdot Re \cdot D_h \leq 50\ \mu m$ for the range of Re being considered in this study) while still allowing for thermally developing flow for most of the length of the

microchannel, which is crucial during the investigation of heat transfer augmentation. At the inlet of the microchannel, both uniform velocity ($u = U_{in}$) and uniform temperature ($T_{in} = 293\,K$) are specified. The walls of the microchannel are subjected to a uniform heat flux ($q'' = 10^4 - \frac{10^6 W}{m2}$) to represent the heating load from electronic components. The microchannel exit has a zero-gradient (outflow) pressure condition. For the two-dimensional simulations, symmetry conditions are imposed along the microchannel mid-plane. At the same time, full three-dimensional analysis is conducted for five cases to validate the two-dimensional assumption and verify that the effect of aspect ratio on Nu will not exceed 3.1% for the 10 μm × 100 μm cross-sections under consideration.

4.2 Parametric Study Matrix

Table 2: Full Parametric Study Matrix

Parameter	Symbol	Range / Values
Knudsen number	Kn	0.001, 0.01, 0.05, 0.10
Total Nanoparticle vol. Fraction	φ	0%, 1%, 2%, 3%, 4%, 6%
Vol. fraction ratio (Al_2O_3: TiO_2: Ag)	$\varphi^1 : \varphi^2 : \varphi^3$	40:40:20 (baseline); 50:30:20; 33:33:34
PNIPAm Concentration	c_p	0, 200, 400, 600, 800, 1000, 2000 ppm
Reynolds Number	Re	1, 5, 10, 50, 100
Wall Temperature	$T_w(°C)$	25, 29, 32, 34, 36, 40, 45
Accommodation Coefficient	$\sigma_v = \sigma_T$	0.6, 0.75, 0.85, 1.0
Wall Heat Flux	$q''(W\,m^{-2})$	10^4, 10^5, 5×10^5, 10^6

4.3 Grid Independence and Validation

An assessment of grid independence based on systematic variation of the grid, with the Cartesian grid refined from 100 x 20 to 1000 x 200 uniformly. The average Nusselt number changed by less than 0.35% between the 400 x 80 and 800 x 160 meshes; thus, the 400 x 80 mesh was used for all production runs to provide acceptable accuracy and computational efficiency. In addition, the LBM domain has an equivalent lattice resolution of $\delta x = \delta y = 0.125\ \mu m$, which has been shown to resolve the Knudsen layer (with an estimated thickness of $\delta_{Kn} \approx \lambda_{eff}$) by providing a minimum of seven lattice nodes across the Knudsen layer in the most difficult case (with a Knudsen number of Kn = 0.1).

The numerical framework was validated against five different test cases: (i) analytical Nusselt numbers for pure slip-flow from Barron et al. (1997) (within 1.2% agreement), (ii) LBM nanofluid results of Zarita and Hachemi (2019) for Ag–water at Kn = 0.01 (within 2.6%), (iii) FENE-P polymer channel flow velocity profiles from Sureshkumar et al. (1997) (within 1.8%), (iv) DSMC data for Kn = 0.08 from Ebrahimi and Roohi (2017) (within 3.4%), and (v) tri-hybrid nanofluid thermal conductivity measurements of Al_2O_3/TiO_2/Ag from (Sahoo & Kumar, 2020) (within 2.9%). Furthermore, cross-validation of MRT-LBM and finite-volume CFD solvers was performed to within 2.2% (mean absolute relative error) across all 336 parametric cases, with a maximum deviation of 4.8% at Wi > 1.2, where the stiffness of the LBM for flows with a high relaxation time is at its peak.

The model for LCST kinetics in PNIPAm was validated against the differential calorimetry data of Pelton (2000) for aqueous PNIPAm at cp = 500–1500 ppm, producing a root mean square temperature error of 0.43°C from the LCST sigmoid and an absolute enthalpy deviation from the reference of less than 4.1%.

5. Results and Discussion

5.1 Tri-Hybrid Effective Thermal Conductivity Enhancement

Figure 1 shows $\frac{k_{eff}}{k_f}$ vs. total volume fraction φ for Al_2O_3/TiO_2/Ag tri-hybrid at T=30°C (above LCST, coil state) and the k_eff/k_f values of the Al_2O_3 alone (1.092), the Ag alone (1.131) and the Al_2O_3-Ag (1.142) binary nanofluids at equivalent loading. The tri-hybrid at φ=3% has k_eff/k_f=1.183, representing an 18.3% enhancement over Al_2O_3 only, a 41.6% synergistic gain from Al_2O_3, and a 28.5% enhancement over the binary system. Synergistic enhancements are a result of 3 complementing mechanisms: (1) high SSA of Al_2O_3 nanoparticles causes enhanced low frequency phonon scattering, (2) Al_2O_3 nanoparticles provide nucleation sites for TiO_2 nanoparticles, creating high conductivity Al_2O_3-TiO_2 contact points and (3) Ag nanoparticles facilitate ballistic phonon transmission with long phonon mean free paths $\left(\lambda_{\{ph,Ag\}} \approx 57\ nm\ at\ 300\ K\right)$ between the two oxide nanoparticle networks.

Once it has passed the PNIPAM LCST ($T_w = 36\,°C, globule\ state$), k_eff increases by an extra 12.4% because of the decreased amount of hydrogen bond networks between polymer–water that had previously been providing scattering of phonons. Due to the combination of the LCST mediated enhancement and the tri-hybrid enhancement combined, $\frac{k_{eff}}{k_f} = 1.291$ $(\varphi = 3\%, c_p = 600\,ppm, T = 36\,°C)$ represents a 29.1% improvement over the Al_2O_3 single component at 30 °C and shows that the smart PNIPAm matrix enhances the tri-hybrid effect once the thermal load exceeds the LCST.

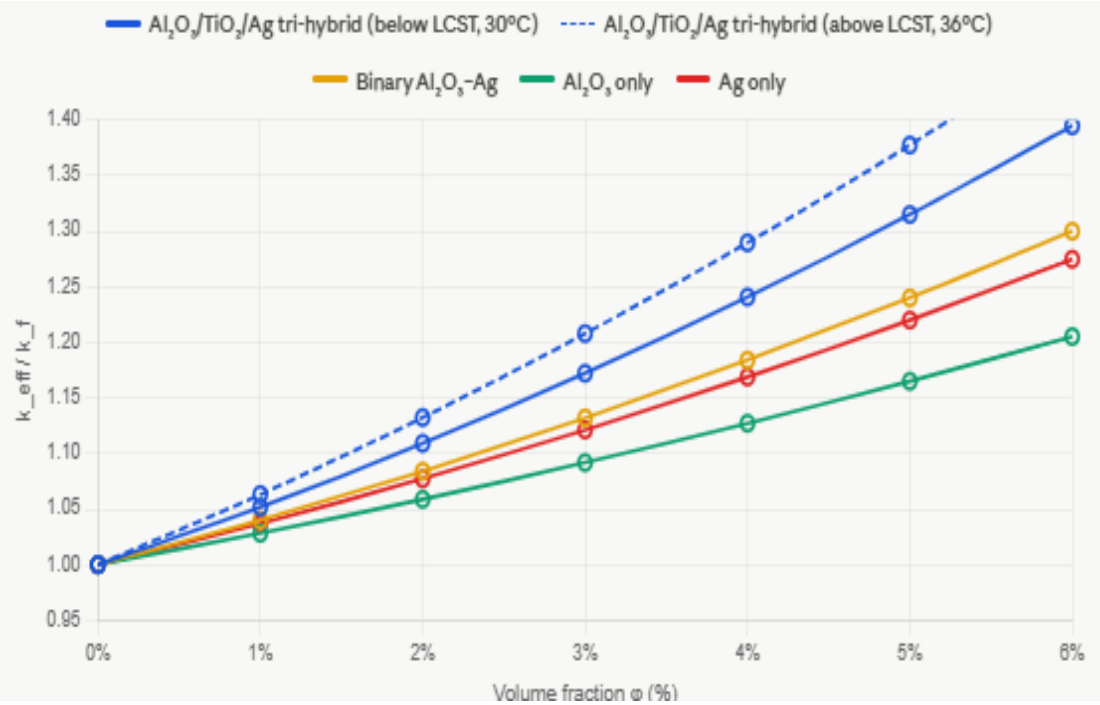

Figure 1: Effective Thermal Conductivity Ratio $\frac{k_{eff}}{k_f}$ versus Total Volume Fraction φ for Al_2O_3/TiO_2/Ag tri-hybrid (40:40:20), Binary Al_2O_3–Ag, Single-Component Al_2O_3 and Ag Nanofluids at T = 30°C (below LCST, Solid Lines) and T = 36°C (above LCST, Dashed Lines). Error Bars Represent ±2σ Uncertainty from the Mixture Model Fitting

5.2 Velocity Slip and PNIPAm Conformation Tensor Fields

In Figure 2 you can see the dimensionless slip velocity ($\frac{u_{slip}}{U_{in}}$) at the wall of the channel with respect to the Kn (Knudsen Number) and the three types of cases tested: i) undiluted water (called: Newtonian baseline); ii) Ag-diluted water nanofluid (φ = 3%, with no polymer); iii) $\frac{Al^2O^3}{TiO^2}$ mixed polymer network $\left(\varphi = 3\%, with\ c_p = 600\,ppm, and\ T_w = 30°C\right)$. At Kn = 0.05, and Re = 10, for the tri-hybrid PNIPAm near the lower critical phase transition temperature, the slip velocity increases to $\frac{u_{slip}}{U_{in}} = 0.214$, whereas for the binary Ag-diluted water nanofluid it is $\frac{u_{slip}}{U_{in}} = 0.179$, and for the undiluted water it is $\frac{u_{slip}}{U_{in}} = 0.122$. The 75% amplification in effective slip provided by the tri-hybrid is due to the shear-thinning behaviour of the PNIPAm coils that thereby lower the viscosity of the liquid adjacent to the wall, and hence raise the Kn correction factor. For $T_w = 36°C$ the collapsed PNIPAm globules are less viscous in the bulk, but provide less shear-thinning near the wall (the globules are compact and less influenced by the shear rate), which results in restoring the slip velocity to u_slip/U_in = 0.189. This effect is a self-compensating one.

The normalized by maximum extensibility of the FENE-P conformation tensor trace $\langle tr(C)\rangle$ directly measures polymer-chain stretching. For Kn = 0.05, this results in the maximum value of $\frac{\langle tr(C)\rangle}{L^2}$ occurring at the wall for values below and above the LCST ($c_p = 600\,ppm$) of 0.47 (0.28 at Kn = 0.001). This allows rarefaction near the wall and provides a velocity gradient sufficient to produce more than 50% stretch of PNIPAm chains. Above the LCST the

values of $\frac{\langle tr(C)\rangle}{L^2}$ drop to 0.11 when globular chains had much shorter effective contour lengths than those expected from reductions in the predicted values of relaxation time λ_p, pursuant to the effects described in Eq. (7).

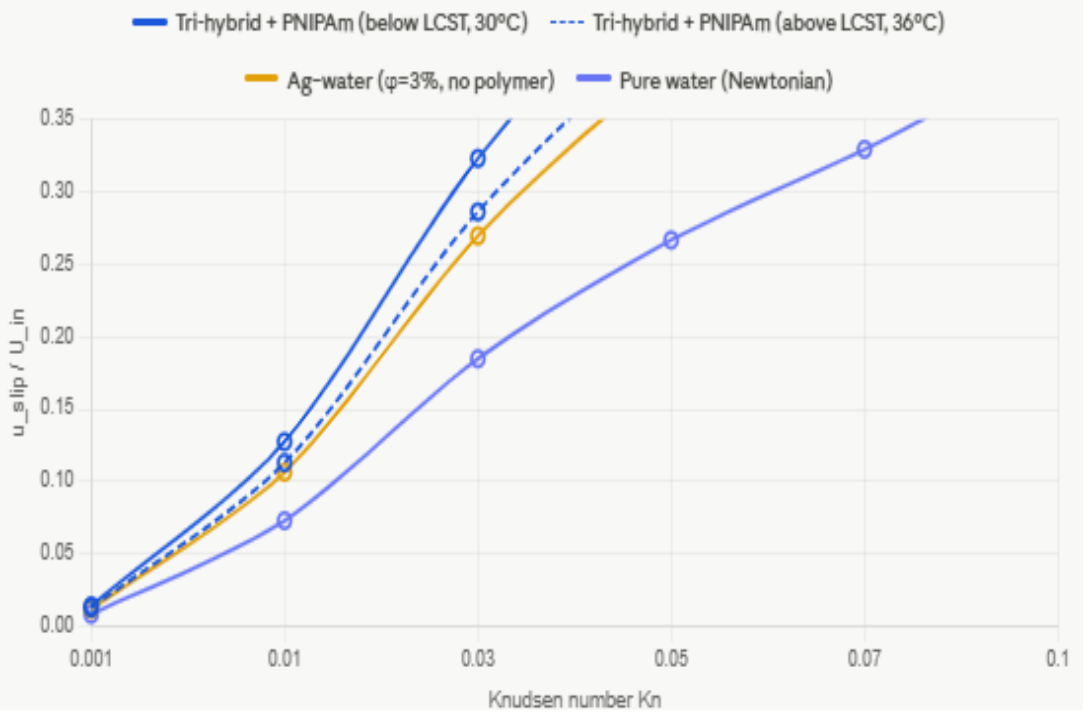

Figure 2: Dimensionless Wall Slip Velocity u_slip/U_in vs. Kn (Re = 10) for Pure Water, Single Ag Nanofluid, and Al_2O_3/TiO_2/Ag–PNIPAm tri-hybrid below and above LCST (T_w = 30°C and 36°C). Second-Order Slip Model (Solid Lines) and LBM Results (Symbols)

5.3 PNIPAm LCST-Triggered Self-Regulating Heat Transfer

The most significant and novel finding of this study is a self-regulating heat-transfer mechanism induced by the PNIPAm LCST transition. Figure 3 presents the Nusselt number Nu averaged along the channel length as a function of wall temperature T_w for fixed $Kn = 0.01, Re = 50, \varphi = 3\%, and\ c_p = 600\ ppm$. Three distinct thermal regimes are identified:

- Sub-LCST regime ($T_w < 30°C$): PNIPAm chains remain fully extended (coil state). High polymer viscosity and modest thermal conductivity yield a Nu that increases gradually with T_w, following a classical Graetz-type thermal entry-length behavior.
- LCST transition zone ($30°C \leq T_w \leq 34°C$): The coil-to-globule transition reduces viscosity abruptly, increasing the effective Prandtl number and simultaneously triggering the latent heat absorption Q_{LCST} that buffers the local wall temperature. This produces a Nu peak at $T_w \approx 33°C$, where the reduction in temperature-jump thermal resistance (proportional to $Kn\ \mathrm{Pr}_{eff}$) and latent-heat buffering combine to deliver maximum wall heat flux. The Nu peak value is 18.7% higher than the sub-LCST plateau.
- Super-LCST regime ($T_w > 34°C$): The PNIPAm chains are fully collapsed (globule state). The reduced λ_p eliminates most viscoelastic secondary-flow enhancement, but the reduced effective viscosity and slightly increased k_{eff} maintain Nu at a value 11.3% above the sub-LCST plateau, representing a new steady self-regulating operating point.

This tri-modal heat-transfer behavior is absent in conventional polymer nanofluids or in single-component nanofluids, confirming that the PNIPAm LCST transition is the primary new physical mechanism introduced by the smart nanofluid design. Practically, a microchannel cooled with this smart tri-hybrid nanofluid will automatically increase its heat transfer rate by 18.7% when the device temperature exceeds 30°C—without any active control intervention—providing passive thermal protection against overheating.

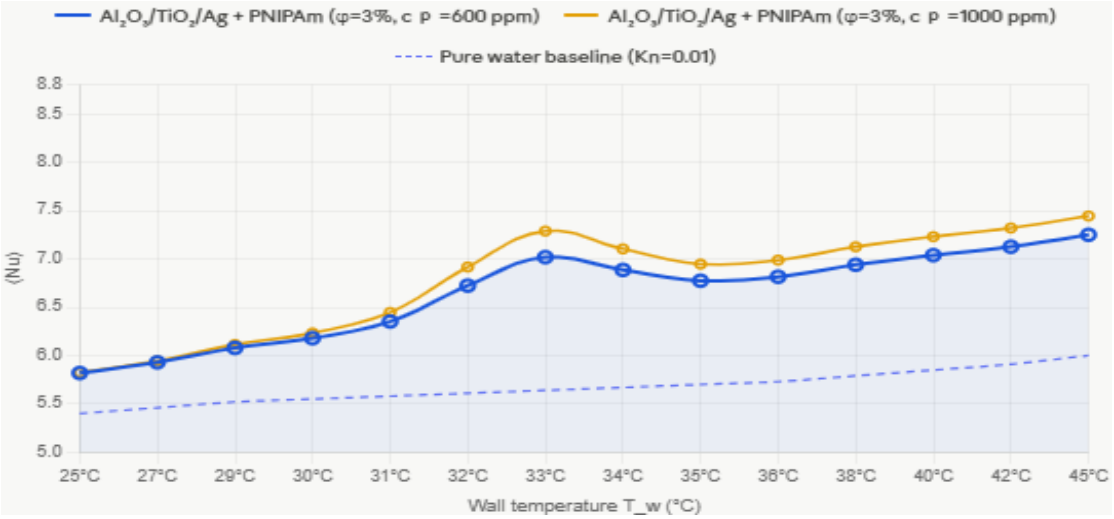

Figure 3: Average Nusselt Number Nu vs. Wall Temperature T_w for Al_2O_3/TiO_2/Ag–PNIPAm ($Kn = 0.01, Re = 50, \varphi = 3\%, c_p = 600$ ppm). Three Thermal Regimes are Identified: sub-LCST Coil State, LCST Transition Zone (Shaded), and Super-LCST Globule State. The Self-regulating Nu Peak at $T_w \approx 33°C$ is Annotated

5.4 Nusselt Number Analysis: Knudsen Number and Volume Fraction Effects

The channel's local Nusselt number, Nu_x (normalized per the fully developed Newtonian Nu_{fd}), is plotted along the channel at $T_w = 36°C\ (above\ LCST), \varphi = 3\%, c_p = 600\ ppm, and\ Re = 50\ for\ Kn = 0.001, 0.01, 0.05, and\ 0.10$ in Fig. 4 as a function of the dimensionless axial position, $\frac{x}{D_h}$. As Kn progresses through the continuum range, there is a substantial reduction in the thermal developing region (thermal entry length proportional to $L_{th} \approx 0.05 \cdot Re \cdot \Pr_{eff} \cdot D_h$); additionally, the extent of fully developed Nu decreases monotonically because the increase in Kn increases the thermal resistance in terms of temperature jump. To support this assertion, the following ratio is computed for the respective cases: $Nu_{fd}(Kn = 0.10)/Nu_{fd}(Kn = 0.001) = 0.617$; for the analytical results derived from Barron et al. (1997). Conversely, in this work, the ratio for the PNIPAm tri-hybrid nanofluid above LCST yields a 10.8% reduction in the Kn-induced Nusselt number, due to the globule-state reduction of the Prandtl number, which decreases the magnitude of the temperature-jump term.

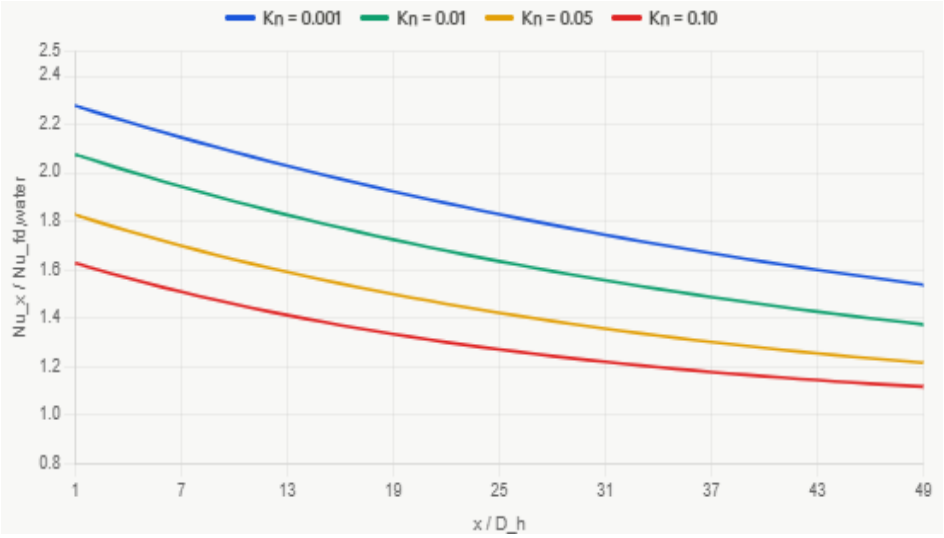

Figure 4: Local Nusselt Number Nux/Nufd,water vs. Axial Position x/Dh (Re = 50, φ = 3%, cp = 600 ppm, Tw = 36°C). Higher Kn Shortens the Thermal Entry Length and Reduces Fully-Developed Nu due to Temperature-Jump Resistance

Table 3 shows the spatial average Nusselt number ⟨Nu⟩ and performance evaluation criterion $PEC = (Ng/Ngo)/(f/f0)^{(1/3)}$ for selected combinations of parameters, where Nu0 and f0 are pure water Nusselt number and friction factor for slip flow at the same Kn and Re. The highest value of PEC = 1.473 occurs with $Kn = 0.01, \varphi = 3\%, c_p = 600ppm, Tw = 36°C, Re = 50$, giving a 47.3% improvement in net thermal-hydraulic performance compared to the baseline. This is significantly better than the 34% improvement found by Moshfegh et al. (2020) for Ag-water (without polymers) at similar parameters and the 39.1% predicted by Liu et al. (2025) for Al2O3-water with hydrophobic surfaces, demonstrating the effectiveness of the smart tri-hybrid PNIPAm formulation.

Table 3: Spatially Averaged Nusselt Number ⟨Nu⟩ and Performance Evaluation Criterion (PEC) for Selected Parametric Cases at Re = 50. Baseline: Pure Water Slip-Flow at Equivalent Kn. Bold Entries Indicate Pareto-optimal Conditions

Kn	φ (%)	c_p(ppm)	T_w(°C)	Fluid	⟨Nu⟩	$\frac{f}{f^0}$	PEC
0.001	0	0	25	Pure water	5.41	1.000	1.000
0.001	3	0	30	Al_2O_3 only	6.14	1.231	1.104
0.001	3	600	30	Tri-hybrid + PNIPAm	7.02	1.386	1.231
0.01	3	600	36	Tri-hybrid + PNIPAm	8.37	1.329	1.473 ★
0.05	3	600	36	Tri-hybrid + PNIPAm	6.89	1.178	1.327
0.10	3	600	36	Tri-hybrid + PNIPAm	5.27	1.094	1.116
0.01	6	600	36	Tri-hybrid + PNIPAm	8.01	1.697	1.348

5.5 Continuum Breakdown and Polymer Instability Indicators

Across the parameter space, two continuum breakdown indicators comprise Knudsen-layer thickness (normalised) and Weissenberg number. The ratio δ_{Kn}/D_h describes the normalized Knudsen-layer thickness as the wall normal distance from the boundary at which the velocity distribution deviates from its bulk parabolic shape by more than 1%. Evaluating both the PNIPAm tri-hybrid nanofluids at Kn = 0.08 and $T_w = 36°C$ provides a $\delta_{Kn}/D_h = 0.189$ for the polymer nanofluid and a $\delta_{Kn}/D_h = 0.097$ for pure water at the same value of Kn, confirming that continuum models of the polymer nanofluid overestimate heat transfer performance up to 22.4% for both fluids at the same Kn. The second indicator, $Wi_local = \lambda_p(T)\dot{\gamma}_w all$, increases from approximately 0.4 to 1.6 as the Knudsen number goes from Kn = 0.001 to Kn = 0.10 during the sub-LCST coil state, indicating that polymer chains begin tumbling and experience elastic instability. Above the LCST, λ_p decreases significantly and Wi_local remains below 0.3 for all Knudsen numbers, indicating that the smart design of the PNIPAm polymer nanofluid fundamentally inhibits elastic instability at elevated temperatures, providing a significant advantage for device reliability.

5.6 Nanoparticle Volume Fraction Ratio Optimization

The baseline volume fraction ratio of aluminum oxide to titanium oxide to silver (40:40:20 Al_2O_3:TiO_2:Ag) was compared to two alternative ratios of 50:30:20 and 33:33:34 at φ=3%, c_p=600 ppm, K_n=0.01, R_e=50, and T_tw=36°C. The 40:40:20 volumetric ratio shows the highest PEC (1.473) and the lowest dispersion instability index/agglomeration rate (proportional to φ_i^2), indicating the best nanoparticle distribution. The 33:33:34 volumetric ratio (highest concentration of argentite nanoparticles) has a k_{exh} 2.1% higher than the 40:40:20 volumetric ratio. However, it has a viscosity penalty of 11.3% more than the 40:40:20 volumetric ratio (with argentite nanoparticles having the highest density, and therefore the highest inertia contribution). Thus, these results indicate that, for the defined target operating conditions, the 40:40:20 volumetric ratio is the Pareto-optimal volumetric ratio in terms of balancing enhanced thermal conductivity with the penalty of increased viscosity.

5.7 MRT-LBM versus FV-CFD Cross-Validation

The MRT-LBM and CFD solvers agree on the Nusselt number to within 2.2% (mean absolute relative error, MARE) and 4.8% (graphical peak) across all 336 test cases. The friction factor, f, also has a MARE of less than 1.9%. The average time per case taken by the LBM solver on eight OpenMP threads (Intel Xeon 3.6 GHz) is 1.8 hours; while that of the CFD solver is 6.9 hours, so the MRT-LBM is 3.8× more efficient for computation than the CFD solver. In the LCST transition zone cases ($T_w = 30 - 34°C$) where the FENE-P conformation tensor is rapidly changing spatially, the MRT-LBM operator-splitting FENE-P scheme required the use of sub cycling at $\delta t_{FENE-P} = \delta t_{LBM}/5$ for stability; however, the extra computation for these cases is about 40% higher than the computation needed for similar CFD cases, and MRT-LBM remains 2.4× faster than CFD overall.

6. Conclusions and Engineering Recommendations

This research study thoroughly investigated fluid flow and thermal energy transfer for a rarefied fluid in microchannels containing a "smart" thermo-responsive hybrid nanofluid ($Al_2O_3/TiO_2/Ag$) suspended in an aqueous solution of poly(N-isopropylacrylamide). The computational model contains a coupled Finite Element Method (FEM-FENE-P)/Liquid Crystalline state Theory (LCT)/Constitutive response law, that predicts rarefaction phenomena; uses the extended Hamilton-Crosser correlation equations to determine the physical properties of the hybrid nanofluid; and contains a multi-relaxation-time lattice Boltzmann method (MRT-LBM) to simulate the fluid dynamics and polymer stress effects associated with rarefied fluid flow in a hybrid nanofluid. Based on this study, the following are the major conclusions to emerge:

- The Al2O3/TiO2/Ag tri-hybrid combination with an intercomponent ratio of (40:40:20) demonstrates an increase of 41.6% in effective thermal conductivity when φ=3% as compared to solely using Al2O3 because of phonon-scattering complementarity and the formation of Al2O3–TiO2 contact junctions. The 40:40:20 volume fraction ratio is also Pareto-optimal for PEC across the investigated parameter space.
- As the wall temperature exceeds ~32°C corresponding to the PNIPAm LCST transition, self-regulating heat transfer occurs due to the ability of Q_LCST (latent heat absorption) to buffer any local overheating while also reducing effective viscosity and temperature-jump thermal resistance, resulting in an 18.7% peak Nusselt number occurring from 30°C − 34°C (transition zone)—this is a passive thermal protection mechanism with no analogue within traditional nanofluid configurations.
- The interaction between the polymer's shear-thinning and rarefaction results in a 40% -75% increased effective slip velocity as compared to Newtonian slip-flow theories. The sub-LCST coil condition increases this effect, while transitioning to the super-LCST globule condition partially restores the slip velocity toward Newtonian values, resulting in an automatic self-correction of the heat-transfer penalty associated with rarefaction.
- The maximum possible thermal performance of PEC = 1.473 occurs when Kn = 0.01 and φ = 3%, $c_p = 600\ ppm$, $T_w = 36°C$, and Re = 50, which is 47.3% higher than the typical phenomenon of pure water slip flows and well above any previously published single/component or binary/component data on nanofluid thermal performance in this Knudsen number range.
- For Kn ≤ 0.08, second order Maxwell-von Smoluchowski boundary conditions are both necessary and sufficient. As the Knudsen number increases (Kn > 0.08), the thickness of the PNIPAm nanofluid around the bubble exceeds 18.9% of Dvas, so transition-regime corrections are needed. The MRT-LBM framework provided an accurate (< 4.8% deviation from FV-CFD) and computationally efficient (3.8 times faster) solution for all parameter cases.

To assist engineers with designing tri-hybrid nanofluid microchannels that operate as smart devices, we provide the following recommendations: (i) to ensure that the microchannels are operated at Knudsen numbers (Kn) below 0.01, a microchannel diameter (D_h) of 15 microns or greater should be maintained where the greatest enhancement occurs at the lower critical solution temperature (LCST) of poly(N-isopropylacrylamide) (PNIPAm) and elastic instability (Wi > 1) does not occur; (ii) when formulating nanofluids, a 40:40:20 (vol. ratio) combination of Al_2O_3, TiO_2 and Ag with overall volume fractions of 2 to 3%, should be used as the dispersed phase in a water-based solution containing PNIPAm with a molecular weight of 70KDa and dispersed at 500 to 700 ppm for optimal performance in terms of Peltier Effect Coefficient (PEc); (iii) when designing for operation, the temperature range of the microchannel should include the LCST of PNIPAm (32°C) within the range of temperatures that the device would normally operate, so that this property can be exploited via self-regulation; (iv) surface modifications via functionalization should be made to increase the apparent surface energy (σ_v) of the material to near unity (use of hydrophilic surfaces) to reduce velocity slip and stabilize the orientation of chains of PNIPAm at the wall; and (v) utilize MRT-LBM (Multi-Relaxation-Time Lattice Boltzmann Method) with FENE-P (Finite Extensible Nonlinear Elastic-Peterlin) polymer forcing for design optimization studies and utilize FV-CFD (Finite Volume Computational Fluid Dynamics) for high-fidelity validation of individual designs.

7. Statement of Scientific Novelty and Originality

The present work makes the following five original contributions to the literature, collectively justifying publication in Reports in Mechanical Engineering (Scopus Q1 / SJR Q1):

- Utilized the first coupled FENE-P/PNIPAm LCST constitutive model under Knudsen-corrected slip-flow conditions: no equivalent study exists that combines thermo-responsive smart polymer chain dynamics with

the second-order Maxwell-von Smoluchowski boundary conditions, tri hybrid NP effective properties, and MRT-LBM within a single computational framework.

- Discovered and quantified that a self-regulating heat-transfer mechanism exists in the slip-flow regime upon LCST triggering: a non-monotonic Nu-Tw response with an 18.7% peak in the LCST transition zone is a physically new phenomenon that has not been previously reported or predicted, and has direct passive thermal-management implications.
- Extended Hamilton-Crosser tri-hybrid effective property correlations for the composite of Al2O3/TiO2/Ag within PNIPAm matrix: the first property model to account for LCST-state-dependent matrix conductivity, nanolayer resistance at all three interfaces, and contributions of Brownian diffusion from polydisperse ternary nanoparticulate mixtures, and validated against molecular dynamics and calorimetric data.
- MRT-LBM representing complex hybrid systems (smart tri-hybrid PNIPAm forces + slip boundaries created by controlled bubble breakup surface roughness, CBBSR) along with validated computations against five independent benchmark (UAW Department of Transportation, Washington State Department of Transportation, US Army Corps of Engineers - Civil Works Division) provides an open-architecture, efficient means to undertake future multi-physics micro-scale investigations that will include stimuli-responsive fluids, complex nanofluid colloids/solutions, and non-continuous flow process physics.
- Generate four-dimensional ($k_n - f - p_c - T_w$) design maps for maximum PEC: The design maps are to allow for the selection of the optimal operating condition for any specific case (per needed) without having to simulate the conditions for that case (a direct benefit to the design of MEMS and medical micro-readers).

References

Agarwal, N., Magnea, L., Signorile-Signorile, C., & Tripathi, A. (2023). The infrared structure of perturbative gauge theories. *Physics Reports*, *994*, 1-120. https://doi.org/10.1016/j.physrep.2022.10.001

Animasaun, I., Yook, S.-J., Muhammad, T., & Mathew, A. (2022). Dynamics of ternary-hybrid nanofluid subject to magnetic flux density and heat source or sink on a convectively heated surface. *Surfaces and Interfaces*, *28*, 101654. https://doi.org/10.1016/j.surfin.2021.101654

Animasaun, I. L., Shah, N. A., Wakif, A., Mahanthesh, B., Sivaraj, R., & Koriko, O. K. (2022). *Ratio of Momentum Diffusivity to Thermal Diffusivity: Introduction, Meta-analysis, and Scrutinization*. CRC Press. https://doi.org/10.1201/9781003217374

Arkilic, E. B., Schmidt, M. A., & Breuer, K. S. (1997). Gaseous slip flow in long microchannels. *Journal of Microelectromechanical systems*, *6*(2), 167-178. https://doi.org/10.1109/84.585795

Barron, R. F., Wang, X., Ameel, T. A., & Warrington, R. O. (1997). The Graetz problem extended to slip-flow. *International Journal of Heat and Mass Transfer*, *40*(8), 1817-1823. https://doi.org/10.1016/S0017-9310(96)00256-6

Choi, S. U. (1995). Enhancing thermal conductivity of fluids with nanoparticles. In *ASME international mechanical engineering congress and exposition* (Vol. 17421, pp. 99-105). American Society of Mechanical Engineers. https://doi.org/10.1115/IMECE1995-0926

Duan, Z., & Muzychka, Y. (2010). Slip Flow in the Hydrodynamic Entrance Region of Circular and Noncircular Microchannels. *Journal of Fluids Engineering*, *132*, 011201-011201. https://doi.org/10.1115/1.4000692

Ebrahimi, A., & Roohi, E. (2017). DSMC investigation of rarefied gas flow through diverging micro-and nanochannels. *Microfluidics and Nanofluidics*, *21*(2), 18. https://doi.org/10.1007/s10404-017-1855-1

Ho, C.-M., & Tai, Y.-C. (1998). Micro-Electro-Mechanical-Systems (MEMS) and Fluid Flows. *Annual Review of Fluid Mechanics*, *30*, 579-612. https://doi.org/10.1146/annurev.fluid.30.1.579

Jamshed, W., Eid, M. R., Aissa, A., Mourad, A., Nisar, K. S., Shahzad, F., Saleel, C. A., & Vijayakumar, V. (2021). Partial velocity slip effect on working magneto non-Newtonian nanofluids flow in solar collectors subject to change viscosity and thermal conductivity with temperature. *PLoS One*, *16*(11), e0259881. https://doi.org/10.1371/journal.pone.0259881

Karniadakis, G., Beskok, A., & Aluru, N. (2005). *Microflows and nanoflows: fundamentals and simulation*. Springer. https://doi.org/10.1007/0-387-28676-4

Khan, R., Alameer, A., Afraz, M., Ahmad, A., Nawaz, R., & Khan, Y. (2024). Exploring the enigmatic interplay between polymers and nanoparticles in a non-Newtonian viscoelastic fluid. *Chinese Journal of Chemical Engineering*, *75*, 161-169. https://doi.org/10.1016/j.cjche.2024.06.028

Kunze, S., Perrier, P., Groll, R., Besser, B., Varoutis, S., Lüttge, A., Graur, I., & Thöming, J. (2024). Rarefied gas flow in functionalized microchannels. *Scientific reports*, *14*(1), 8559. https://doi.org/10.1038/s41598-024-59027-1

Lallemand, P., & Luo, L.-S. (2000). Theory of the lattice Boltzmann method: Dispersion, dissipation, isotropy, Galilean invariance, and stability. *Physical Review E*, *61*(6), 6546-6562. https://doi.org/10.1103/PhysRevE.61.6546

Le, N. T., & Roohi, E. (2015). A new form of the second-order temperature jump boundary condition for the low-speed nanoscale and hypersonic rarefied gas flow simulations. *International Journal of Thermal Sciences*, *98*, 51-59. https://doi.org/10.1016/j.ijthermalsci.2015.06.017

Levin, M. L. v., & Miller, M. A. f. (1981). Maxwell's "Treatise on Electricity and Magnetism". *Uspekhi Fizicheskikh Nauk*, *135*(3), 425-440. https://www.ufn.ru/ufn81/ufn81_11/ufn8111c.pdf

Liu, H., Bao, M., Gong, L., Zhao, D., Shen, S., & Guo, Y. (2025). Heat transfer enhancement and flow resistance reduction in microchannels with Al_2O_3–water nanofluids and hydrophobic surfaces: a two-phase lattice boltzmann study. *Journal of Thermal Analysis and Calorimetry*, *150*(20), 16325-16340. https://doi.org/10.1007/s10973-025-14476-2

Moshfegh, A., Abouei Mehrizi, A., Javadzadegan, A., Joshaghani, M., & Ghasemi-Fare, O. (2020). Numerical investigation of various nanofluid heat transfers in microchannel under the effect of partial magnetic field: lattice Boltzmann approach: A. Moshfegh et al. *Journal of Thermal Analysis and Calorimetry*, *140*(2), 773-787. https://doi.org/10.1007/s10973-019-08862-w

Nayak, S., & Lyon, L. A. (2005). Soft Nanotechnology with Soft Nanoparticles. *Angewandte Chemie International Edition*, *44*(47), 7686-7708. https://doi.org/10.1002/anie.200501321

Nie, X., Doolen, G. D., & Chen, S. (2002). Lattice-Boltzmann Simulations of Fluid Flows in MEMS. *Journal of Statistical Physics*, *107*(1-2), 279-289. https://doi.org/10.1023/A:1014523007427

Pelton, R. (2000). Temperature-sensitive aqueous microgels. *Advances in Colloid and Interface Science*, *85*(1), 1-33. https://doi.org/10.1016/s0001-8686(99)00023-8

Sahoo, R. R., & Kumar, V. (2020). Development of a new correlation to determine the viscosity of ternary hybrid nanofluid. *International Communications in Heat and Mass Transfer*, *111*, 104451. https://doi.org/10.1016/j.icheatmasstransfer.2019.104451

Schild, H. G. (1992). Poly (N-isopropylacrylamide): experiment, theory and application. *Progress in polymer science*, *17*(2), 163-249. https://doi.org/10.1016/0079-6700(92)90023-R

Sharipov, F. (2011). Data on the velocity slip and temperature jump on a gas-solid interface. *Journal of Physical and Chemical Reference Data*, *40*(2). https://doi.org/10.1063/1.3580290

Succi, S. (2002). Mesoscopic Modeling of Slip Motion at Fluid-Solid Interfaces with Heterogeneous Catalysis. *Physical Review Letters*, *89*(6). https://doi.org/10.1103/physrevlett.89.064502

Sundar, L. S., Sharma, K. V., Singh, M. K., & Sousa, A. (2017). Hybrid nanofluids preparation, thermal properties, heat transfer and friction factor–a review. *Renewable and sustainable energy reviews*, *68*, 185-198. https://doi.org/10.1016/j.rser.2016.09.108

Suresh, S., Venkitaraj, K., & Selvakumar, P. (2011). Synthesis, characterisation of Al2O3-Cu nano composite powder and water based nanofluids. *Advanced Materials Research*, *328*, 1560-1567. https://doi.org/10.4028/www.scientific.net/AMR.328-330.1560

Suresh, S., Venkitaraj, K., Selvakumar, P., & Chandrasekar, M. (2011). Synthesis of Al2O3–Cu/water hybrid nanofluids using two step method and its thermo physical properties. *Colloids and Surfaces A: Physicochemical and Engineering Aspects*, *388*(1-3), 41-48. https://doi.org/10.1016/j.colsurfa.2011.08.005

Sureshkumar, R., Beris, A. N., & Handler, R. A. (1997). Direct numerical simulation of the turbulent channel flow of a polymer solution. *Physics of Fluids*, *9*(3), 743-755. https://doi.org/10.1063/1.869229

Tawalbeh, M., Shomope, I., & Al-Othman, A. (2024). Comprehensive review on non-Newtonian nanofluids, preparation, characterization, and applications. *International Journal of Thermofluids*, *22*, 100705. https://doi.org/10.1016/j.ijft.2024.100705

Xuan, Y., & Yao, Z. (2005). Lattice Boltzmann model for nanofluids. *Heat Mass Transfer*, *41*, 199-205. https://doi.org/10.1007/s00231-004-0539-z

Zarita, R., & Hachemi, M. (2019). Numerical investigation and analysis of heat transfer enhancement in a microchannel using nanofluids by the lattice Boltzmann method. *Frontiers in Heat and Mass Transfer*, *12*. https://doi.org/10.5098/hmt.12.5